Accepted Manuscript

Facile mechanochemical synthesis of non-stoichiometric silica-carbon composite for enhanced lithium storage properties

Bo Zhang, Hongwei Wang, Chang Liu, Dejun Li, Hyun-Kyung Kim, Chris Harris, Cheng-yen Lao, Amr Abdelkader, Kai Xi

PII: S0925-8388(19)32172-3

DOI: https://doi.org/10.1016/j.jallcom.2019.06.101

Reference: JALCOM 50999

To appear in: *Journal of Alloys and Compounds*

Received Date: 19 October 2018

Revised Date: 23 May 2019

Accepted Date: 8 June 2019

Please cite this article as: B. Zhang, H. Wang, C. Liu, D. Li, H.-K. Kim, C. Harris, C.-y. Lao, A. Abdelkader, K. Xi, Facile mechanochemical synthesis of non-stoichiometric silica-carbon composite for enhanced lithium storage properties, *Journal of Alloys and Compounds* (2019), doi: https://doi.org/10.1016/j.jallcom.2019.06.101.

Facile mechanochemical synthesis of non-stoichiometric silica-carbon composite for enhanced lithium storage properties

Bo Zhang[*a,b] , Hongwei Wang[a,b], Chang Liu[a,b], Dejun Li[a,b], Hyun-Kyung Kim[c], Chris Harris [c], Cheng-yen Lao [c], Amr Abdelkader [c,d], Kai Xi[*c]

[a] Energy & Materials Engineering Centre, College of Physics and Materials Science, Tianjin Normal University, Tianjin 300387, China.

[b] Tianjin International Joint Research Centre of Surface Technology for Energy Storage Materials, Tianjin 300387, China

[c] Department of Materials Science and Metallurgy, University of Cambridge, Cambridge CB3 0FS, United Kingdom

[d] Department of Design and Engineering, Faculty of Science & Technology, Bournemouth University, Poole, Dorset, BH12 5BB, United Kingdom.

∗Corresponding author. E-mail: zhangbo2014@ tjnu.edu.cn (B. Zhang);

kx210@cam.ac.uk (K. Xi).

Highlights

- Non-stoichiometric silica-carbon composite was prepared by mechanochemical method.
- The heat generation assisted the fusion of nanoparticles into 3D porous structure.
- The structure facilitated shortening diffusion path, alleviating volume expansion.
- Partial reduction, homogenous distribution ensured excellent electric conductivity.
- The composite with high performance and low cost is a promising candidate of anode.

- **TOC graphic**

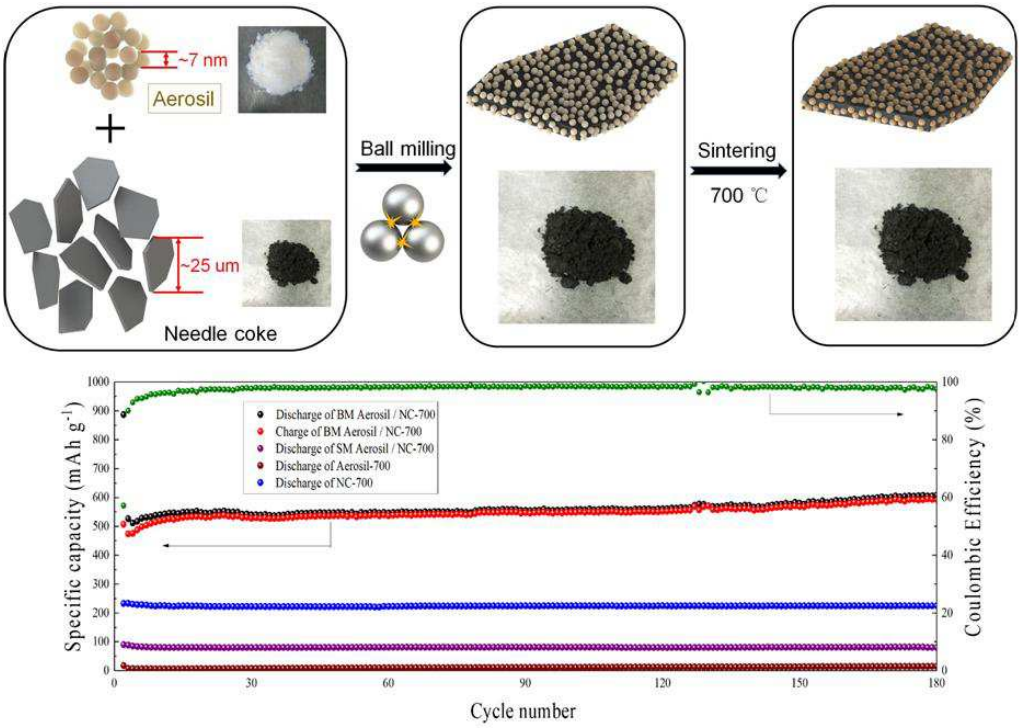

Abstract

A large number of new electrode materials and novel structural designs are emerging for lithium-ion batteries, yet scalable synthesis and raw material costs still hinder the practical

application of such materials. Here, we designed and fabricated a low-cost SiO_x/C composite by a facile and scalable mechanofusion route with a ball-milling method. We selected aerosil and graphite precursor-needle coke, which are two widely used materials in industry, as a silicon source and carbon source, respectively. This SiO_x/C composite shows a high reversible capacity (ca. 550 mAh g^{-1}) at the 180th cycle and good rate performance. Our scalable synthesis route of electrode materials can stimulate the progress of other energy storage technologies for practical applications.

Keywords

lithium ion batteries, mechanofusion, aerosil, needle coke, Si-based anodes.

1 Introduction

Lithium-ions batteries (LIB_S) are not only widely used in portable devices but also important for applications in electric vehicles and smart grids. There are increasing demands on lighter and smaller LIBs, which can be achieved by increasing the capacity of electrode materials. The conventional graphite anode has a limited theoretical specific capacity of 372 mAh g^{-1} which is

difficult to satisfy the current demand[1,2]. Silicon has received much attention as an alternative anode material in next-generation LIBs s, due to its high theoretical specific capacity (about 4200 mAh g^{-1}) and relative abundance in nature[3]. However, silicon anode suffers from poor cycle life due to substantial volume changes (as high as 300%)[4] during repeated charging and discharging[5]. Several strategies have been proposed to improve the cyclic stability, including but not limited to the use of nanoparticles[6], form alloys or composites with other elements[7] or carbon coating[8-10]. Amongst them, silicon nanoparticles can most efficiently alleviate the considerable volume changes, but still, the high production cost in nanoparticles limits the practicality. Recently, silica-derived materials have attracted considerable attention as an anode for LIBs. For example, Chang et al.[11] used commercial SiO_2 powder (Quartz, Aldrich, 325 mesh) as a raw material to prepare the LIB anode, which exhibited a reversible capacity of 800 mAh g^{-1} over 200 cycles. Lv et al.[12] synthesized porous silica particles coated with an amorphous carbon film using tetraethoxysilane (TEOS) as the source of silica followed by ball milling in ethanol. Guo et al.[13] prepared an amorphous composite with a reversible capacity of 600 mAh g^{-1} after 12 cycles via a hydrothermal method. Yao et al.[14] used a simple solid-liquid mixed method to prepare a SiO_x/C composite material, showing an initial discharge capacity of 536 mAh g^{-1} and a reversible capacity of 500 mAh g^{-1} at the 50th cycle. During the charging process, amorphous silica and lithium ions react to generate lithium orthosilicate, lithium disilicate and nano-size silicon[13]. As in most ceramic-based electrodes, the silica-derived electrodes suffer from poor cyclic performance due to the low conductivity[13]. Furthermore, the charging mechanism involves the reaction between amorphous silica and lithium to generate lithium orthosilicate, lithium disilicate and nano-size silicon[13,14]. Although this mechanism may help to reduce the distortion by sudden volumetric expansion, the repeated phase changes significantly reduce the cycle life of the electrode[14]. Adding carbonaceous materials to the electrode and using nano-silica have been reported to overcome both the phase changes and the conductivity problem[15]. The carbon materials act as major active sites for lithium ion intercalation and as a buffer to the stress generated by the volume and phase changes[13,15]. However, adapting this solution is impractical due to the complicated process[11-14] of preparing the silica nanoparticles and obtaining a homogeneous dispersion of the carbon materials. Therefore, a more straightforward synthetic method and more advanced material structure are still awaited for the silica-based electrodes to find their way to commercial LIBs.

Ball milling is an old metallurgical process that has been traditionally used for blending powders or reducing the particles size[16]. It has been proven as a powerful technique to produce controlled compositions and sized powders with a homogeneous structure in different systems, which is difficult to obtain with other methods[17]. The mechanical power of the ball mill has been used to drive many chemical reactions and accelerate kinetically slow processes in what is known as mechanochemical processes[18]; These mechanochemical processes are relatively low-cost techniques that have been used on a large-scale nanomaterials production[19].

In this work, a simple mechanochemical synthesis route was employed to partially reduce silica and form a porous network of metallic-like particles embedded in a carbon matrix. The process used aerosil as a cheap silica precursor and needle coke particles as the source of carbon. The heat generated from the milling process induced self-fusion between the non-stoichiometric silica particles, adding another sustainable factor to the advantages of the process. The SiO_x/C composites electrode shows a high reversible capacity, robust cycle stability and excellent rate-capability as an anode material for lithium-ion batteries.

2 Experimental

2.1 Preparation of SiO_x/C core-shell composite

The fabrication process of SiO_x/C core-shell composites is illustrated in Scheme 1. Needle coke (0.3 g) and aerosil (0.7 g) were placed into an agate jar (80 cm^3) with agate balls (30 g, 4 mm in diameter)., The mixture was ball-milled with high energy mechanical milling (QM-QX2) (HEMM) at a constant rotation speed of 500 rpm for 12 h at room temperature. The mixture was then sintered at 700 ℃ for 2 h under a flow of argon to give the final composite (denoted as BM Aerosil/NC-700). For comparison, we have prepared a controlled sample by heating a mixture of aerosil and needle coke after gentle mixing using mortar and pastel (donated as SM Aerosil/NC-700). We also separately prepared pure carbon and SiO_2 from heated needle coke and pure aerosil at the same conditions and denoted them as NC-700and Aerosil-700,

respectively. Lastly, a SiO_2 control sample (99.99%, metals basis, 200-mesh) was used for comparison.

2.2. Materials Characterization

The crystal structures of the samples were determined by XRD analysis using Bruker D8a. The surface morphology of the particles was characterized by using a scanning electron microscope (SEM, HITACHI SU8010) with energy dispersive spectroscopy (EDS) and a transmission electron microscope (TEM, JEOL JEM-3000F). For recording the FTIR spectra of the samples, we used a Fourier transform infrared spectroscopy (FTIR, SHIMADZU IRAffinity-1) in the range 400-4000 cm^{-1}. The carbon content of the composites was confirmed using a thermogravimetric analyser (TGA, Pyris Diamond6000 TG/DTA, PerkinElmer Co, America). X-ray photoelectron spectroscopy (XPS, VG ESCALAB MK II) experiments were used for determining the elemental composition of the composite materials.

2.3. Electrochemical characterization

The electrode was prepared by mixing the active material (80 wt. %), acetylene black (10 wt. %) and polyvinylidenefluoride (10 wt. %), with N-methyl-2-pyrrolidone as a solvent. This was spread onto copper foil as a current collector and then dried overnight in a vacuum oven at 80 ℃. The electrodes were then punched into 8 mm diameter discs, with a mass of around 1 mg. For testing the electrochemical performance of the composite materials, the coin cells (CR2032 3 V) were assembled in an argon-filled glove box, where both moisture and oxygen contents were less than 0.1 ppm. Metallic lithium was used as the counter electrode, and porous polypropylene (Celgard 2400) was used as a separator. The electrolyte consisted of 1M $LiPF_6$ in a non-aqueous solution of ethylene carbonate (EC), ethyl methyl carbonate (EMC) and dimethyl carbonate (DMC) with a volume ratio of 1:1:1. The electrochemical performance of the composite materials was tested by galvanostatic charge-discharge tests using Arbin battery cycler (BT2000), Cyclic Voltammetry and Electrochemical Impedance Spectroscopy measurements were conducted using Princeton Applied Research VersaSTAT4 potentiostat. The galvanostatic charge-discharge tests were performed at various current densities of 100、200、400、800 mA g^{-1} in the potential range from 0.001 to 3.0 V. Cyclic Voltammograms were conducted in the voltage range of 0.001-3.0 V at a scan rate of 0.1 mV s^{-1}. Electrochemical Impedance Spectroscopy was carried out in the frequency region of 100 kHz to 0.01 Hz with a perturbation voltage of 5 mV.

3 Results and discussion

The X-ray diffraction patterns of pure NC-700 and pure aerosil-700 are shown in Figure 2a (i, iii), in which the diffraction peaks located in 26° (0 0 2) and 43° (1 1 0)[20] can be attributed to the crystalline graphitic carbon. The two broad peaks at around 30° and 42° are due to the amorphous characteristics of aerosil[14]. The XRD pattern of the BM Aerosil/NC-700 composite overlaps with those of both needle coke and aerosil, indicating that homogeneous mixing occurred between the components of the SiO_x/C composites. Moreover, no peaks of SiC and Si were observed, confirming that the SiO_2 nanoparticles have not been fully reduced[14]. The BET measurements of needle coke, aerosil and composite after mechanochemical synthesis were also conducted to investigate the coating effect by ball milling. As can be seen from the results, the BET surface area of BM Aerosil/NC-700 composite decreased to 127.6 m^2/g after coating aerosil (198.6 m^2/g) on needle coke (**2.4** m^2/g) by mechanochemical method. The type of N_2 adsorption/desorption isotherms is not changed before and after mechanochemical synthesis as showed in Fig. S2.

Despite the XRD results, the XPS scanning of the Si 2p peak in the composite materials shows a sign of a partial reduction. As can be seen from Figure 2d, the Si 2p peak can be fitted with four distinctive peaks: the peak at 103.05 eV is attributed to SiO_2 (Si^{4+})[24], while the other peaks, located at 100.6 eV, 101.2 eV and 101.85 eV, are attributed to the other oxidation states of silicon Si^{0+}, Si^{2+}, Si^{3+} respectively[25-28]. By our calculations, the content of Si^{4+} in the composite accounts for about 16%, on the other hand, the contents of Si^{0+}, Si^{2+} and Si^{3+} account for about 26%, 27 % and 31%, respectively. The results of the C1s peak also show a sign of Si-C bond after milling and calcination. Figure 2e shows that the C 1s can be fitted by three peaks; the one at ~284 is for the Sp^2 carbon, the peak at ~282 is on the position of the C-Si bond, and the peak at higher binding energy could be for the C-O bonds. These results are similar to that reported for the oxycarbide phases[42,43]. These kinds of mixed phases are very difficult to be detected by XRD, due to the overlaps in the peaks positions[44].

The surface chemistry of the prepared particles was investigated further by FTIR. The FTIR spectra of the BM Aerosil/NC-700, BM Aerosil/NC composite and commercial SiO samples are shown in Figure 2b. The spectrum of the commercial SiO has three peaks at 1089.7 cm^{-1}, 786.9 cm^{-1} and 457.1 cm^{-1} that can be assigned to the Si-O rocking vibration, the symmetric Si-O-Si stretching vibration and the asymmetric Si-O-Si stretching vibration[21,22], respectively. After milling and calcination, the spectrum of the BM Aerosil/NC-700 composites samples kept the characteristic peaks of the Si-O bond suggesting the siloxane network of the commercial SiO has been maintained[23]. Compared to the commercial SiO, the intensity of the peaks for BM Aerosil/NC-700 composite is weaker due to the lower O/Si ratio in SiO_x/C composites than that of SiO[14]. In addition to the Si-O bond's peaks, there are two peaks appeared after calcination at ~ 1053 cm^{-1} and 1220 cm^{-1}, which may be assigned to the C-O stretching vibration[13-15]. The appearance of the C-O bonds on the surface of the Aerosil/NC-700 particles further support the formation of the Si-O-C compound.

To study the effect of the synthesis process on the morphology of the aerosol we used electron microscopic techniques. The SEM images of NC-700 and BM Aerosil/NC-700 powders are shown in Figure 1a, 1b. The heat-treated aerosol, sample NC-700, showed flake-like particles with clear straight edges and size distribution of ca.10-20 μm. Ball-milling for 12 hours destroyed the ordered structures of the flakes, and the BM Aerosil/NC-700 sample exhibits irregular shapes of the micron-sized powder (Figure 1c). The particles have more round edges suggesting that the particles are more metallic, possibly due to the partial reduction. The particles also seem to sinter together by the effect of the heat generated during the ball milling. Furthermore, the composite particle size is apparently smaller than the needle coke size. The TEM images of the BM Aerosil/NC-700 (Figure 1e and Figure 1f) revealed that the particles size is as small as 20 nm aggregated in micron-sized clusters. This kind of aggregated nanoparticles is usually very porous, which may facilitate the ions transfer process at the electrode/electrolyte interface of the BM Aerosil/NC-700. Elemental scanning using energy-dispersive X-ray spectrometry (EDX) reveals the presence of C, O, and Si. The elemental mapping of the three elements is represented in Figures 1g-j. The locations of the silicon, oxygen and carbon are roughly overlapping, further proving the formation of the oxycarbide phase composite.

A more profound study of the reaction mechanism was carried out by electrochemical methods. The cyclic voltammogram of the BM Aerosil/NC-700 electrode is presented in Figure 3b. The first cycle of the CV curve has two peaks in the cathodic scan and another two peaks in the anodic scan. The first cathodic peak (i) appears at around 0.75 V, corresponding to the decomposition of the electrolyte solution and the formation of the solid electrolyte interface (SEI) layer[29]. The other cathodic peak (ii) at around 0.2 V is due to the chemical reactions between lithium ions and the SiO_2 particles. The two anodic peaks can be attributed to the delithiation of the $Li_2Si_2O_5$, Li_4SiO_4 compounds and the reduction of the amorphous SiO_2 nanoparticles (or the Si-O sites in the oxycarbide phase) [13,15]. Moreover, it should be noted that an anodic peak at around 0.3 V (iii) can be observed, which is due to the partial reversibility of $Li_2Si_2O_5$ to SiO_2 and $Li_{15}Si_4$ to Si[11]. Due to the complex nature of the electrode materials, the delithiation process is taking place in more than one step. The reaction between lithium ions and SiO_2 can be summarized as follows[26,27]:

$$2SiO_2 + 4Li^+ + 4e^- \rightarrow Li_4SiO_5 + Si \quad (1)$$

$$SiO_2 + 4Li^+ + 4e^- \rightarrow 2Li_2O + Si \quad (2)$$

$$5SiO_2 + 4Li^+ + 4e^- \leftrightarrow 2Li_2Si_2O_5 + Si \quad (3)$$

$$4Si + 15Li^+ + 15e^- \leftrightarrow Li_{15}Si_4 \quad (4)$$

As expressed in Eqs. (1) and (2), the newly formed Li_4SiO_5 and Li_2O might consume some lithium ions, resulting in irreversible capacity in the process of discharging. On the other hand, the newly formed nano-silicon can be dispersed in Li_4SiO_5 and Li_2O uniformly, which can effectively relieve the volume expansion effect, ensuring the high reversible capacity of the composite during repeated charge and discharge processes[32]. The above equations are also valid for SiO_x because the non-stoichiometric SiO_x is composed with SiO_2 and SiO, which is partially reduced from aerosil(SiO_2). Likewise, the amorphous SiO is formed with amorphous Si and SiO_2-like clusters as well as unique interface domains[33].

Figure 3a displays the charge-discharge curve of the first three cycles of composite materials at a current density of 100 mA g^{-1}. The composite exhibits an initial discharge capacity of 887.2 mAh g^{-1} and a charge capacity of 507.4 mAh g^{-1} with an initial coulombic efficiency of 57.19 %. The reversible capacity of the composite is much higher than that of the carbon materials (372 mAh g^{-1})[14]. Figure 3c shows the cycle performance of BM Aerosil/NC-700、NC-700、SM Aerosil/NC-700 and Aerosil-700 composites. At a current density of 100 mA g^{-1}, the reversible specific capacity of the BM Aerosil/NC-700 composite material is about 550 mAh g^{-1} even after 180 cycles, indicating high reversibility and excellent cycle stability. Furthermore, the coulombic efficiency of BM Aerosil/NC-700 composite maintains efficiency of 97.9% from the 2nd cycle. On the other hand, the specific capacity of the heated needle coke is only 220 mAh g^{-1}, and that of the pure aerosil heated at 700℃ is as low as 10 mAh g^{-1} due to their poor conductivity. The SM Aerosil/NC-700 composite prepared by the simple mixing of aerosil and needle coke materials in mortar has a capacity of 80 mAh g^{-1} at a current density of 100 mA g^{-1}. The enhanced electrochemical performance of BM Aerosil/NC-700 is attributed to the unique structure of the composite, in which needle coke provides not only efficient electron and Li^+ transportation, but also accommodate the volume expansion during lithination[34]. Interestingly, the specific capacity of the composite BM Aerosil/NC-700 slightly increased during the first few cycles. It is generally believed that the silica crystal size diminishes during the repeated lithium ion insertion/extraction process, leading to a shorter diffusion path of the lithium ion and higher utilization of silica[35,36], thereby, achieving higher reversible specific capacity[37]. The composite of BM Aerosil/NC-700 also exhibits excellent rate capability at various rates as shown in Figure 3d. When the current density is gradually increased from 100 mA g^{-1} to 800 mA g^{-1}, the specific capacity of the composite material is ca. 550 mAh g^{-1}, 480 mAh g^{-1}, 450 mAh g^{-1}, and 390 mAh g^{-1}, respectively. Upon decreasing the current density back to 100 mA g^{-1}, a specific capacity of 520 mAh g^{-1} is recovered, displaying outstanding rate performance.

To further explore the reasons for the exceptional electrochemical performance of the BM Aerosil/NC-700 composite, EIS was employed to examine the interfacial impedance. Figure 4 shows the Nyquist plots of BM Aerosil/NC-700 composite and the SM Aerosil/NC-700

composite electrode after different cycles. The semicircle in the high-frequency region can be assigned to the charge transfer resistance (Rct), and the line in the low-frequency region is attributed to the diffusion impedance (Warburg impedance)[38]. Due to the overlapping between the SEI film and the charge transfer impedance, a depressed semicircle in the high-frequency is presented range after several cycles[39,40]. For the BM Aerosil/NC-700 composite electrode, the semicircles representing the charge-transfer resistance (Rct) are much smaller than that of the SM Aerosil/NC-700 composite materials after the 1st, 5th and 10th cycles, as displayed in Figure 4a-c. Moreover, the Rct of the BM Aerosil/NC-700 composite has almost no noticeable change from the 5th to the 10th cycle, as shown in Figure 4d, owing to the stable interfacial impedance of the unique structure of the composite[20]. The charge-transfer resistance is decreased with the temperature increased from 600□ to 800□ due to higher carbonization of green needle coke as shown in Fig. S4. It is well known that charge-transfer resistance in cells has a negative impact on their capacity[41]. The unique structure of the BM Aerosil/NC-700 composite prepared by ball-milling facilitates interfacial charge transfer and Li^+ diffusion, leading to better performance than that of the composite prepared by simple mixing.

4 Conclusions

In summary, a low-cost SiO_{2-x}/C composite was prepared by a simple mechanochemical method. The process made maximum utilization of the energy by using the heat generated during the ball milling to fuse the nanoparticles into a 3D porous structure. This novel porous structure played an important role in shortening the diffusion pathway and alleviating of the volume expansion during the lithiation step. The partial reduction in the silica and the homogenous distribution of the carbon in the composite ensured an excellent electric conductivity, which significantly improved the cyclic performance of the anode. As an anode material for lithium-ion batteries, this composite presents excellent cycling stability and large reversible capacity of about 550 mAh g^{-1} after 180 cycles. Also, when current density increases to 800 mA g^{-1}, the discharge capacity of this composite is still as high as 390 mAh g^{-1}, showing excellent rate performance. Considering the low-cost of the raw materials and the simplicity of the synthesis process, this new SiO_x/C composite is a promising candidate as an anode for lithium-ion batteries.

ACKNOWLEDGMENT

This work was financially supported by R&D project (0620301-53H16023) for Li batteries by Anshan Xingde Material Technology Corporation.

REFERENCES

[1] Tarascon J M, Armand M. Issues and challenges facing rechargeable lithium batteries. Materials For Sustainable Energy, 2010: 171-179.

[2] Sato K, Noguchi M, Demachi A, et al. A mechanism of lithium storage in disordered carbons. Science, 1994, 264(5158): 556-558.

[3] Son S B, Trevey J E, Roh H, et al. Microstructure study of electrochemically driven LixSi. Advanced Energy Materials, 2011, 1(6): 1199-1204.

[4] Beaulieu L Y, Hatchard T D, Bonakdarpour A, et al. Reaction of Li with alloy thin films studied by in situ AFM. Journal of the Electrochemical Society, 2003, 150(11): A1457-A1464.

[5] Peng K, Jie J, Zhang W, et al. Silicon nanowires for rechargeable lithium-ion battery anodes. Applied Physics Letters, 2008, 93(3): 033105.

[6] Green M, Fielder E, Scrosati B, et al. Structured silicon anodes for lithium battery applications. Electrochemical and Solid-State Letters, 2003, 6(5): A75-A79..

[7] Kasavajjula U, Wang C, Appleby A J. Nano-and bulk-silicon-based insertion anodes for lithium-ion secondary cells. Journal of Power Sources, 2007, 163(2): 1003-1039..

[8] Liu Y, Wen Z Y, Wang X Y, et al. Electrochemical behaviors of Si/C composite synthesized from F-containing precursors. Journal of Power Sources, 2009, 189(1): 733-737..

[9] Doh C H, Shin H M, Kim D H, et al. Improved anode performance of thermally treated SiO/C composite with an organic solution mixture. Electrochemistry Communications, 2008, 10(2): 233-237..

[10] Veluchamy A, Doh C H, Kim D H, et al. Improvement of cycle behaviour of SiO/C anode composite by thermochemically generated Li_4SiO_4 inert phase for lithium batteries. Journal of Power Sources, 2009, 188(2): 574-577..

[11] Chang W S, Park C M, Kim J H, Kim Y U, Jeong G, Sohn H J, Quartz (SiO2): a new energy storage anode material for Li-ion batteries. Energy & Environmental Science. 2012, 6895-6899.

[12] Lv P, Zhao H, Wang J, et al. Facile preparation and electrochemical properties of amorphous SiO_2/C composite as anode material for lithium ion batteries. Journal of Power Sources, 2013, 237: 291-294.

[13] Guo B, Shu J, Wang Z, et al. Electrochemical reduction of nano-SiO_2 in hard carbon as anode material for lithium ion batteries. Electrochemistry Communications, 2008, 10(12): 1876-1878.

[14] Yao Y, Zhang J, Xue L, et al. Carbon-coated SiO_2 nanoparticles as anode material for lithium ion batteries. Journal of Power Sources, 2011, 196(23): 10240-10243..

[15] Sun Q, Zhang B, Fu Z W, Lithium electrochemistry of SiO_2 thin film electrode for lithium-ion batteries. Appl. Surf. Sci. 2008, 254(13), 3774-3779.

[16] Zhang D L, Processing of advanced materials using high-energy mechanical milling. Progress in Materials Science. 2004, 49(3-4), 537-560.

[17] Wang C S, Wu G T, Zhang X B, et al. Lithium insertion in carbon-silicon composite materials produced by mechanical milling. Journal of the Electrochemical Society, 1998, 145(8): 2751-2758.

[18] Motozuka S, Tagaya M, Ogawa N, et al. Effective preparation of graphite nanoparticles using mechanochemical solid-state reactions. Solid State Communications. 2014,190, 28-32.

[19] He Y, Shiflet G J, Poon S J. Ball milling-induced nanocrystal formation in aluminum-based metallic glasses. Acta Metallurgica et Materialia, 1995, 43(1): 83-91.

[20] Lv P, Zhao H, Gao C, et al. Highly efficient and scalable synthesis of SiO_x/C composite with core-shell nanostructure as high-performance anode material for lithium ion batteries. Electrochimica Acta, 2015, 152: 345-351.

[21] Kagel R O, Nyquist R A. Infrared Spectra of Inorganic Compounds (3800-45 cm^{-1}s). 1971..

[22] Prud'homme E, Michaud P, Joussein E, et al. Silica fume as porogent agent in geo-materials at low temperature. Journal of the European Ceramic Society, 2010, 30(7): 1641-1648.

[23] Wang J, Zhao H, He J, et al. Nano-sized SiO_x/C composite anode for lithium ion batteries. Journal of Power Sources, 2011, 196(10): 4811-4815..

[24] Xu K, Ben L, Li H, et al. Silicon-based nanosheets synthesized by a topochemical reaction for use as anodes for lithium ion batteries. Nano Research, 2015, 8(8): 2654-2662..

[25] Hohl A, Wieder T, Van Aken P A, et al. An interface clusters mixture model for the structure of amorphous silicon monoxide (SiO). Journal of Non-Crystalline Solids, 2003, 320(1-3): 255-280. .

[26] Park C M, Choi W, Hwa Y, et al. Characterizations and electrochemical behaviors of disproportionated SiO and its composite for rechargeable Li-ion batteries. Journal of Materials Chemistry, 2010, 20(23): 4854-4860. .

[27] Yu B C, Hwa Y, Park C M, et al. Reaction mechanism and enhancement of cyclability of SiO anodes by surface etching with NaOH for Li-ion batteries. Journal of Materials Chemistry A, 2013, 1(15): 4820-4825..

[28] Yin J, Wada M, Yamamoto K, et al. Micrometer-scale amorphous Si thin-film electrodes fabricated by electron-beam deposition for Li-ion batteries. Journal of the Electrochemical Society, 2006, 153(3): A472-A477.

[29] Kasavajjula U, Wang C, Appleby A J. Nano-and bulk-silicon-based insertion anodes for lithium-ion secondary cells. Journal of Power Sources, 2007, 163(2): 1003-1039.

[30] Lu Y, Wang Y, Zou Y, et al. Macroporous Co_3O_4 platelets with excellent rate capability as anodes for lithium ion batteries. Electrochemistry Communications, 2010, 12(1): 101-105.

[31] Lee J I, Choi N S, Park S. Highly stable Si-based multicomponent anodes for practical use in lithium-ion batteries. Energy & Environmental Science, 2012, 5(7): 7878-7882.

[32] Wu X, Shi Z, Wang C, et al. Nanostructured SiO_2/C composites prepared via electrospinning and their electrochemical properties for lithium ion batteries. Journal of Electroanalytical Chemistry, 2015, 746: 62-67.

[33] Hirata1 A, Kohara S, Asada T, Arao M, Yogi C, Imai H, Tan Y, Fujita T, Chen M, Atomic-scale disproportionation in amorphous silicon monoxide. Nature Communications, 2016, 11591.

[34] Ren Y, Wu X, Li M. Highly stable SiO_x/multiwall carbon nanotube/N-doped carbon composite as anodes for lithium-ion batteries. Electrochimica Acta, 2016, 206: 328-336.

[35] Cui L F, Ruffo R, Chan C K, et al. Crystalline-amorphous core−shell silicon nanowires for high capacity and high current battery electrodes. Nano letters, 2008, 9(1): 491-495.

[36] Gao J, Lowe M A, Abruna H D. Spongelike nanosized Mn_3O_4 as a high-capacity anode material for rechargeable lithium batteries. Chemistry of Materials, 2011, 23(13): 3223-3227.

[37] Ju Y, Tang J A, Zhu K, et al. SiOx/C composite from rice husks as an anode material for lithium-ion batteries. Electrochimica Acta, 2016, 191: 411-416.

[38] Bai X, Wang B, Wang H, et al. In situ synthesis of carbon fiber-supported SiO_x as anode materials for lithium ion batteries. RSC Advances, 2016, 6(39): 32798-32803.

[39] Ruffo R, Hong S S, Chan C K, et al. Impedance analysis of silicon nanowire lithium ion battery anodes. The Journal of Physical Chemistry C, 2009, 113(26): 11390-11398.

[40] Li M, Li J, Li K, et al. SiO_2/Cu/polyacrylonitrile-C composite as anode material in lithium ion batteries. Journal of Power Sources, 2013, 240: 659-666.

[41] Mohanty D, Dahlberg K, King D M, David L A, etc. Modification of Ni-Rich FCG NMC and NCA Cathodes by Atomic Layer Deposition: Preventing Surface Phase Transitions for High-Voltage Lithium-Ion Batteries. Scientific Reports, 2016, 6, 26532.

Figure Captions

Scheme 1 The schematic illustrations of synthesis process and composite material.

Table 1 The content of Si valence states by XPS.

Fig. 1 a SEM micrograph of NC-700 powder, **b c** SEM micrograph of BM Aerosil/NC-700 powders before cycle, **d** after 180 cycles and **e f** TEM micrograph of BM Aerosil/NC-700 powders before cycle. **g, h, i, j** EDS elemental mappings of C (blue), Si (yellow), and their overlap.

Fig. 2 a XRD patterns of (□) pure aerosil-700, (□) BM Aerosil/NC-700 and (□) pure NC-700. **b** FTIR spectra of (□) the commercial SiO, (□) the prepared BM Aerosil/NC-700 composite, (□) the prepared BM Aerosil/NC composite before calcination. **c** The TGA curve of as-prepared BM Aerosil/NC composites recorded under Air atmosphere with a heating rate of 10 □ min^{-1}. **d** XPS Si 2p sprctra of BM Aerosil/NC-700 composite materials. **e** XPS C 1s sprctra of BM Aerosil/NC-700 composite materials.

Fig. 3 a The charge–discharge curve at a constant current density of 100 mA g^{-1} and **b** the cyclicvoltammogram of BM Aerosil/NC-700 composite materials of first three cycles at a scan rate of 0.1 mV s^{-1} between 0 and 3.0 V. Electrochemical performance of BM Aerosil/NC-700、NC-700、SM Aerosil/NC-700 and Aerosil-700 composites：**c** cycling performance at a current density of 100 mA g^{-1} and **d** rate-capability of BM Aerosil/NC-700 composite.

Fig. 4 Electrochemical impedance spectra of cells after **a** the first, **b** the 5th cycle, **c** the 10th cycle: BM Aerosil/NC-700 composite materials and SM Aerosil/NC-700 composite materials， and **d** BM Aerosil/NC-700 after different cycles.

Scheme 1

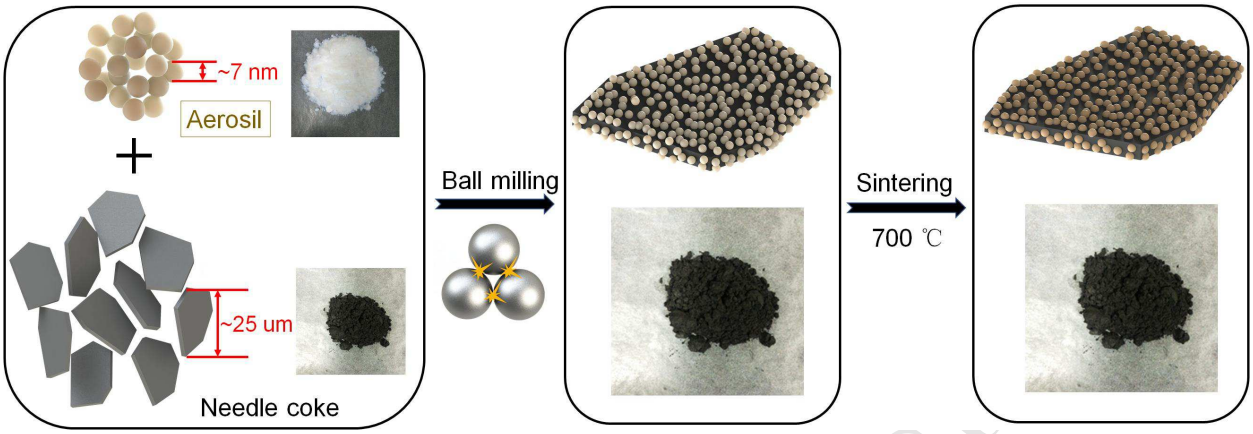

Table 1

valence states	Si^{+}	Si^{2+}	Si^{3+}	Si^{4+}
Content %	26	27	31	16

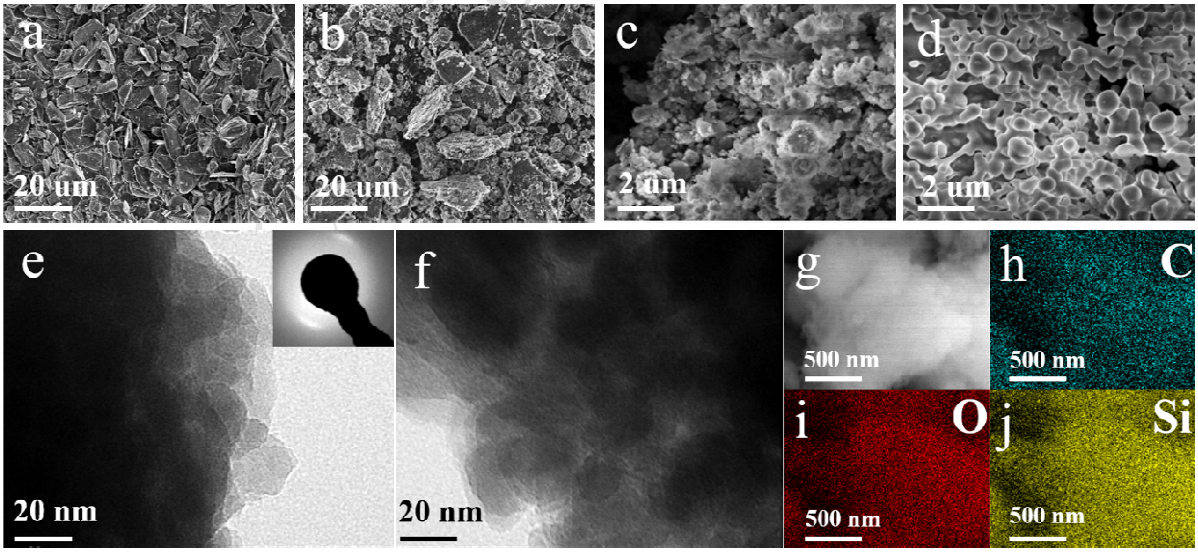

Fig.1

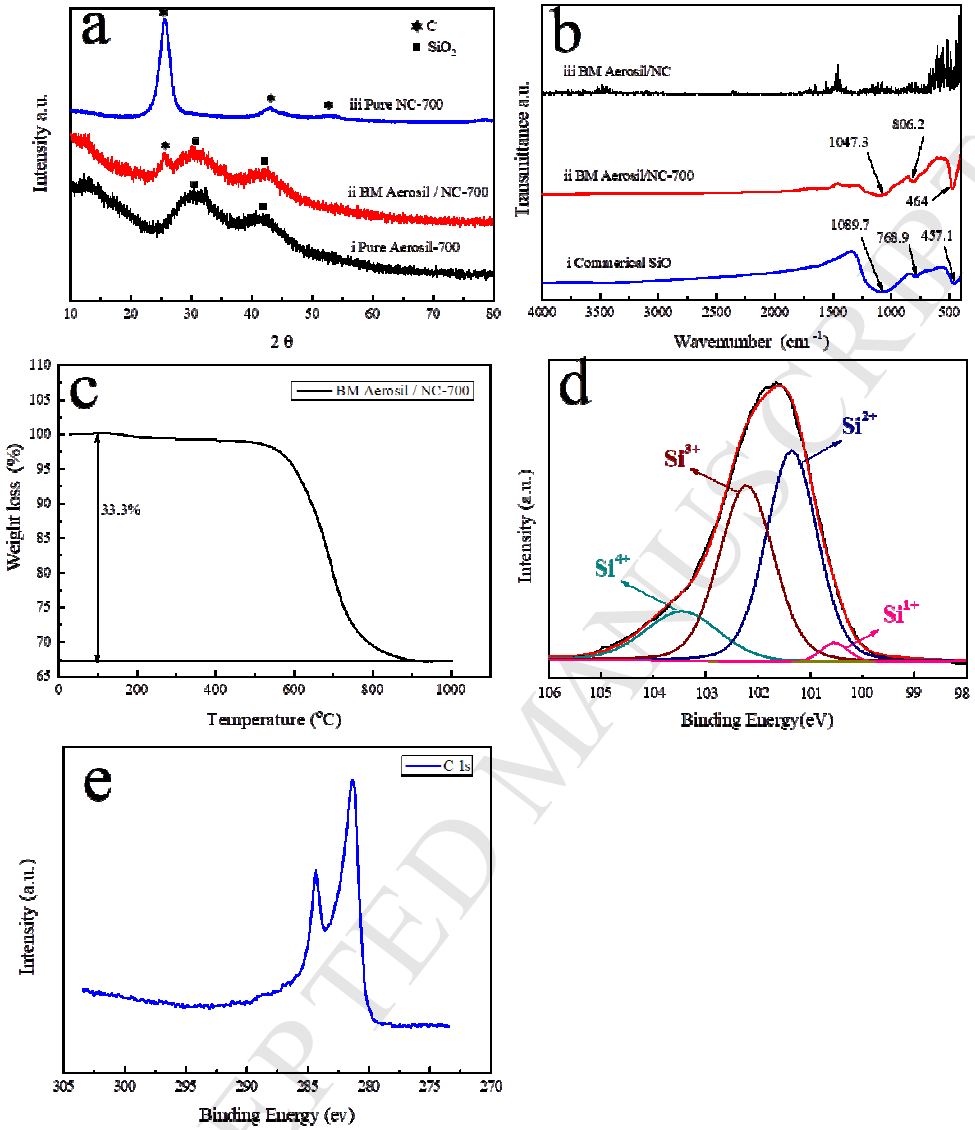

Fig.2

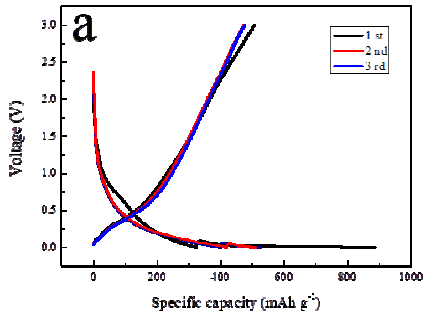

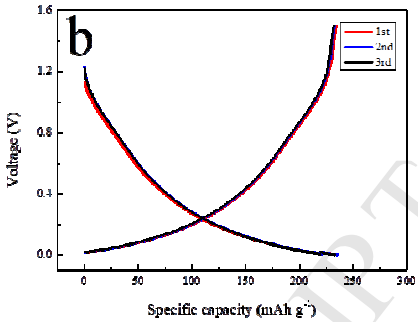

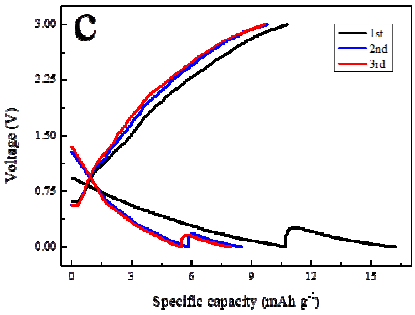

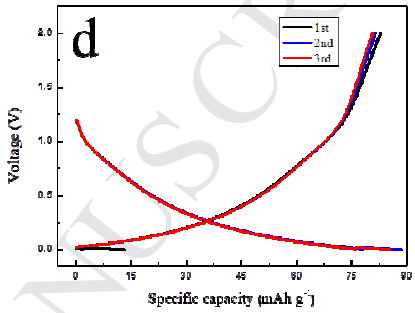

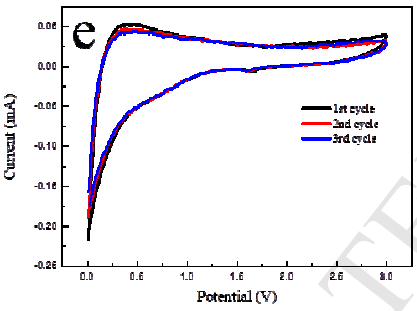

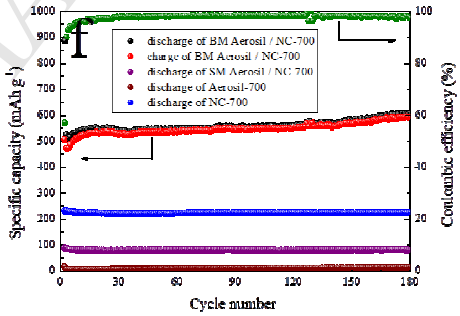

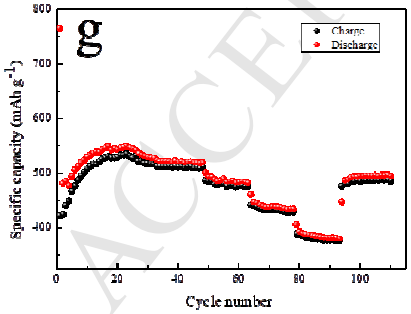

Fig.3

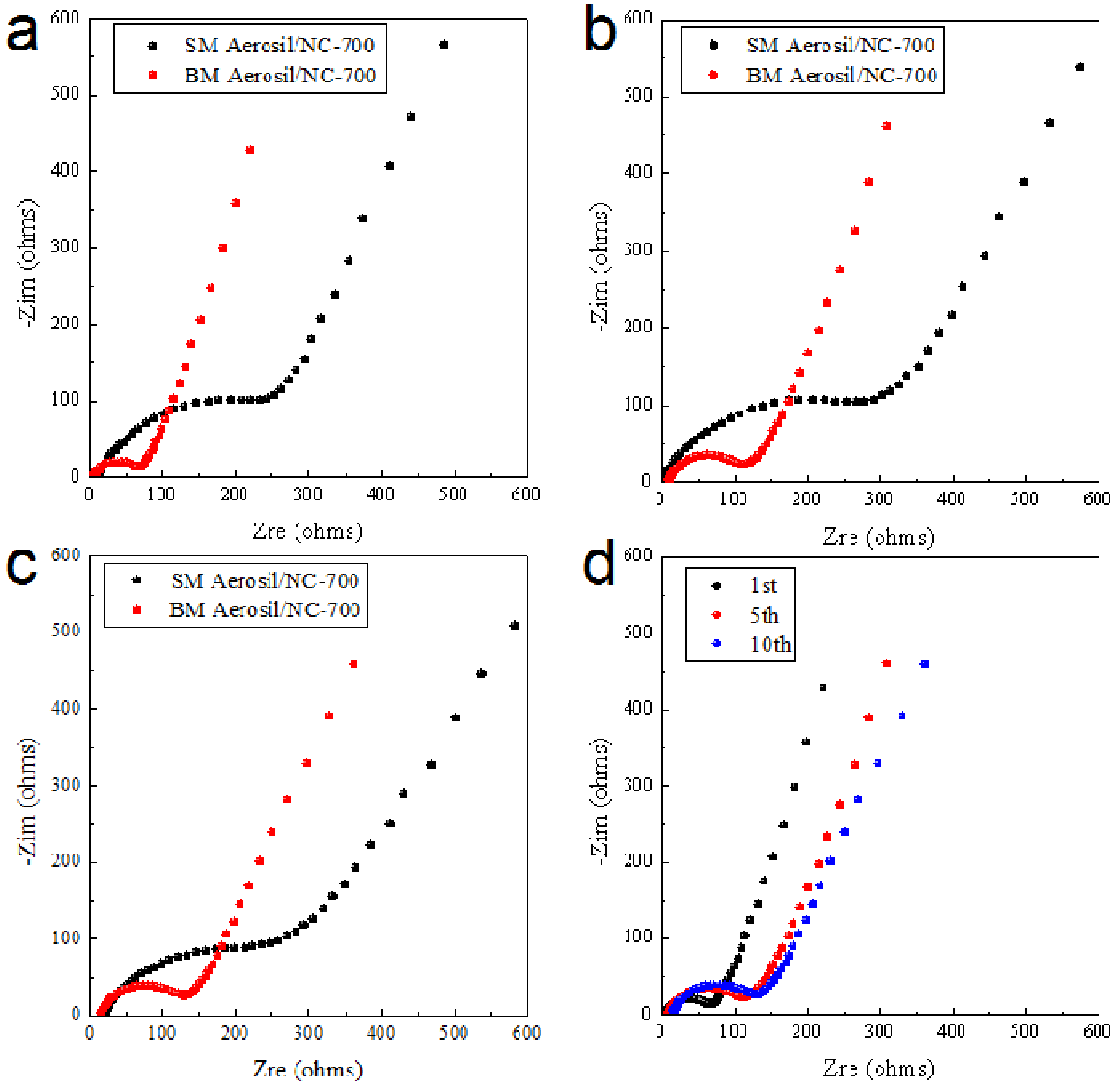
a
SM Aerosil/NC-700
BM Aerosil/NC-700
-Zim (ohms)
Zre (ohms)
b
SM Aerosil/NC-700
BM Aerosil/NC-700
-Zim (ohms)
Zre (ohms)
c
SM Aerosil/NC-700
BM Aerosil/NC-700
-Zim (ohms)
Zre (ohms)
d
1st
5th
10th
-Zim (ohms)
Zre (ohms)

Fig.4